ChemComm

COMMUNICATION

View Article Online
View Journal | View Issue

Cite this: *Chem. Commun.*, 2015, 51, 15657

Received 25th August 2015,
Accepted 4th September 2015

DOI: 10.1039/c5cc07161e

www.rsc.org/chemcomm

Amorphous V_2O_5–P_2O_5 as high-voltage cathodes for magnesium batteries†

Timothy S. Arthur,*[a] Keiko Kato,[a] Jason Germain,[a] Jinghua Guo,[b] Per-Anders Glans,[b] Yi-Sheng Liu,[b] Daniel Holmes,[c] Xudong Fan[d] and Fuminori Mizuno[a]

A deep investigation of amorphous V_2O_5–P_2O_5 powders for magnesium batteries communicates the vital properties to achieving the superior electrochemical performance at a 75 : 25 V_2O_5 : P_2O_5 molar ratio. The manipulation of the inter-layer spacing and amorphization of V_2O_5 can enhance Mg^{2+} diffusion and afford a cathode with high-voltage reversibility.

Multivalent magnesium batteries are viable candidates for post Li-ion technology due to the high volumetric capacity of the Mg metal anode (3833 mA h cm^{-3}), high natural abundance, good safety characteristics and low equilibrium potential (−2.31 V *vs.* hydrogen).[1] The promise of magnesium batteries can only be realized by overcoming two significant hurdles. First, in contrast to lithium metal systems, the chemical/electrochemical reactions at the interface between the Mg metal anode and common electrolytes, such as magnesium perchlorate or magnesium bis(trifluoromethanesulfonyl)imide in acetonitrile, inhibit the magnesium deposition and dissolution because the surface of the anode is passivated. Gregory and Winter,[2] followed by Aurbach *et al.*,[3] found that the passivating layer on the magnesium metal surfaces are non-existent or negligible when a magnesium organoborates and organohaloaluminates are used as the electrolytes. Since, significant improvements in voltage stability, purity, corrosion inhibition and current density have opened the door to search for high voltage, magnesium systems.[4–7] The second major obstacle to realizing a complete Mg battery is the lack of high-voltage cathodes. Due to the divalent nature of Mg^{2+}, high diffusion barriers and slow insertion/de-insertion kinetics have hindered the emergence of viable intercalation cathodes.[8,9] Chevrel-phase $M_xMo_6T_8$ (M = metal and T = S or Se) cathodes were first introduced as excellent prototype systems by Aurbach *et al.* and recent nanoparticle synthesis of Mo_6S_8 by Cheng *et al.*[10] has shown superior capacity, rate and cycle-life. However, the low operating voltage (~1.1 V) of the battery has encouraged further research. A magnesium battery with significant energy density demands high-voltage cathodes to compete with current Li-ion battery technology.

Although years of research have been dedicated to Mg battery cathodes, few impactful advances have been reported in the field. Notably, the emergence of layered V_2O_5 and MoO_3, MoS_2 nanosheets, polyanionic compounds and organic cathodes has renewed confidence in Mg battery cathodes.[11–14] Recently, we have also reported on the importance of determining the magnesiation mechanism of cathodes which exhibit positive electrochemical results.[15] Although the full potential of MnO_2 polymorphs are still being explored, we were encouraged by the electrochemical reversibility exhibited by the amorphous mixture and thus, we considered the rational design of amorphous materials as a possible route to achieve high-voltage Mg battery cathodes.

Amorphous cathodes can provide several advantages for hosting the divalent Mg^{2+} ion. Recent calculations have shown that sluggish diffusion of Mg^{2+} is difficult to overcome in typical transition metal oxide (TMO) cathodes, and the loss of structural integrity of the TMO would hinder continuous and reversible divalent ion intercalation.[9] Amorphous cathodes may enhance reversibility by providing a network capable of absorbing considerable deformations caused by magnesium insertion. In addition, the energy density of the cathode may be vastly improved if a TMO capable of multiple electron transfer is incorporated into the amorphous matrix. Divanadium pentoxide (V_2O_5) is touted as a potential high energy density cathode for battery applications. The capability for vanadium to access multiple oxidation states ($V^{2+} \leftrightarrow V^{5+}$) in addition to a high theoretical capacity and voltage, could also provide benefits for polyvalent ion insertion.

[a] *Materials Research Department, Toyota Research Institute of North America, 1555 Woodridge Ave., Ann Arbor, Michigan 48105, USA. E-mail: tim.arthur@tema.toyota.com*
[b] *Advanced Light Source, Lawrence Berkeley National Lab, One Cyclotron Rd, Berkeley, California 94720, USA*
[c] *Department of Chemistry, Michigan State University, 578 Shaw Lane, East Lansing, Michigan 48824, USA*
[d] *Center for Advanced Microscopy, Michigan State University, 578 Wilson Rd, East Lansing, Michigan 48824, USA*

† Electronic supplementary information (ESI) available: Experimental details and additional results. See DOI: 10.1039/c5cc07161e

For example, $V_2O_5{\cdot}nH_2O$ xerogels, nano-crystalline V_2O_5, and sputtered V_2O_5 thin-films have shown promising results as Mg battery cathodes,[11,16,17] however, the capability of Mg^{2+} to insert into an amorphous form of V_2O_5 is unexplored. A seminal result was first reported by Novàk *et al.*[18] and confirmed by Lee *et al.*,[19] concerning the improvement into layered cathodes, such as V_2O_5, by shielding of the Mg^{2+} with H_2O. However, magnesium batteries containing an aqueous electrolyte media risks decomposition of the Mg metal anode surface. Therefore, our work here will concentrate on the modification of cathodes to improve the electrochemical properties in non-aqueous electrolytes. Previously, the amorphization of V_2O_5 through high-temperature melt-quenching with P_2O_5 has been studied as cathodes for Li-ion batteries,[20] and more recently as a ternary Li_2O–V_2O_5–P_2O_5 complex.[21] Through a thorough analytical investigation, we identify the key elements to form the active component in the amorphous cathode.

The amorphous cathodes were synthesized through planetary ball-milling of V_2O_5 and P_2O_5 powders for 20 h. The resulting dark-to-light brown powders were analyzed with X-ray diffraction (XRD – Fig. 1a). The ratios of $V_2O_5:P_2O_5$ (mol : mol) 85 : 15 to 60 : 40 did not display the presence of any crystalline reflections, indicating the as-made powders are amorphous to XRD. In the high resolution transmission electron microscopy (HR-TEM) image of the 75 : 25 ratio, we did not observe ordering of the lattice (Fig. 1b) and we found similar results for all ratios, supporting the above XRD results. Instead, a halo pattern was observed for all ratios in the selected area electron diffraction. This synthetic method provides a scalable, safe route to form amorphous powders, however it must be noted that complete vitrification of the TMO is best achieved through high temperature melt-quenching.

The new structure of $V_2O_5:P_2O_5$ powders exhibited significant improvements in the electrochemical properties when compared to the parent orthorhombic-V_2O_5. Zhou *et al.* has shown that the insertion of Mg^{2+} into crystalline V_2O_5 is accompanied with a large diffusion barrier,[22] which indicates that manipulation of the structure is essential for V_2O_5-based cathodes. Fig. 1c is cyclic voltammograms (CVs) comparing a milled V_2O_5 cathode and a V_2O_5 : P_2O_5 (75 : 25) cathode. A CV of electrochemically inert SiO_2 is shown to confirm the width of the electrochemical window of the electrolyte and the electrochemical inertness of the conductive carbon and binder. At this point, we cannot completely discount the kinetic influence of the amorphous materials for decreasing the anodic stability of the electrolyte. However, with thorough XPS analysis, we have not been able to observe the decomposition of the ClO_4^- ion on the cathode surface. The CV of the bulk, crystalline V_2O_5 exhibits small cathodic current at low potentials (<1.1 V *vs.* Mg) and two anodic peaks at 2.6 V and 3.1 V *vs.* Mg. The addition of 25 mol% P_2O_5 revealed two notable electrochemical improvements: first, the current density (mA g^{-1}) is significantly increased through the addition of P_2O_5, and second, the presence of an anodic peak at 2.9 V *vs.* Mg demonstrates improved reversibility in the high voltage region. We assign the cathodic current beginning at 1.1 V *vs.* Mg to a reduction of V_2O_5 observed in both the crystalline and amorphous form. The high-voltage reduction/oxidation couple precludes the accurate calculation of the charge through integration of the anodic/cathodic waves. Thus, the electrochemical properties of the cathodes were compared through calculation of the current density (mA g^{-1}) of the oxidation peak potential. Fig. 1d displays the current density of the electrodes as a function of $V_2O_5:P_2O_5$ ratio. Interestingly, the current density of the cathodes finds a maximum value at 75 : 25 signifying that the electrochemical properties are not solely due to the quantity of P_2O_5. Galvanic discharge/charge curves taken at 5 mA g^{-1} rate of the first cycle are shown in Fig. 1e. The improved capacity within the high-voltage region is encouraging, and the initial capacity of 121 mA h g^{-1} with 57 mA h g^{-1} capacity retention up to 5 cycles for the 75 : 25 ratio (Fig. S1a, ESI†). However, extended cycling is hindered by passivation of Mg metal in $Mg(ClO_4)_2/CH_3CN$ electrolytes.[17] Since this is the first report on the magnesiation of amorphous V_2O_5–P_2O_5, we can only compare the initial discharge capacity to sputtered-V_2O_5 (180 mA h g^{-1}),[11] nano-crystalline V_2O_5 (180 mA h g^{-1}),[17] and the lithiation V_2O_5–P_2O_5 (>200 mA h g^{-1}).[20] We are encouraged that through the appropriate nanoscaling of our amorphous materials, we may obtain higher discharge capacities. Through V 2p and Mg 2s XPS (Fig. S1b, ESI†), we have found that magnesium is indeed introduced into the amorphous matrix. The reduction of vanadium is evidenced through the appearance of a shoulder at 514.2 eV of the V $2p_3$ peak coinciding with appearance of a Mg 2s signal at the end of the discharge. The process is partially reversible after the first charge of the cathode. A deep investigation of the reaction mechanism of the amorphous material is

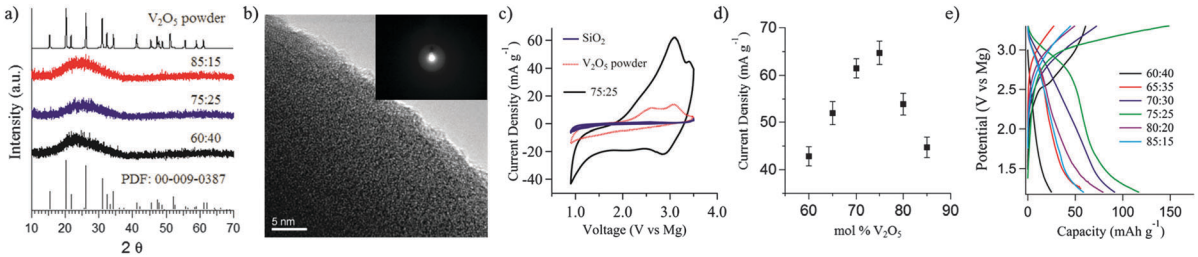

Fig. 1 (a) XRD patterns of representative $V_2O_5:P_2O_5$ powders compared to the commercial V_2O_5 powder. (b) TEM image and SAED pattern (inset) of a $V_2O_5:P_2O_5$ (75 : 25) powder. (c) CVs of a SiO_2, a V_2O_5 powder cathode, and a $V_2O_5:P_2O_5$ (75 : 25) amorphous cathode. Comparison of the (d) current densities (mA g^{-1}) and (e) 1st cycle galvanic curves of $V_2O_5:P_2O_5$ powders.

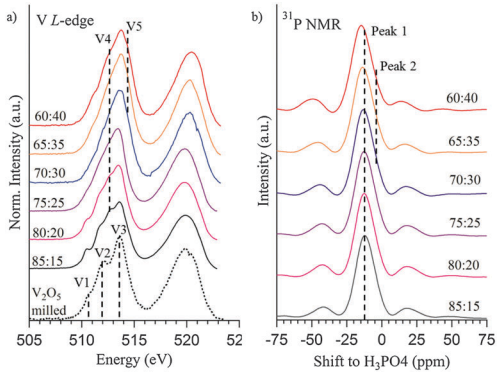

Fig. 2 (a) V L-edge NEXAFS spectra of V_2O_5 : P_2O_5 powders and milled V_2O_5. (b) ^{31}P MAS NMR of V_2O_5 : P_2O_5 powders.

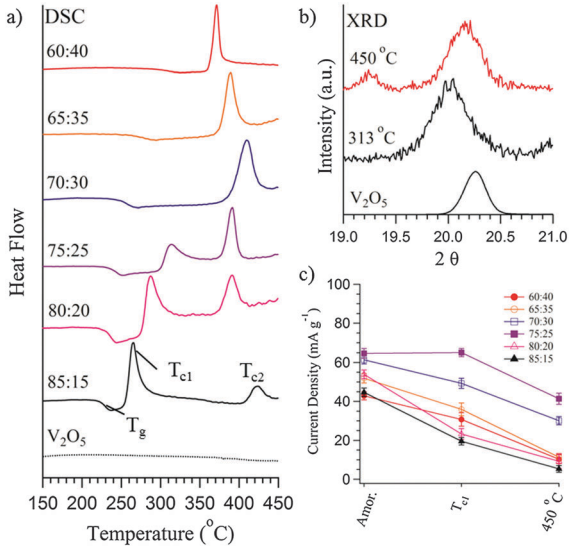

Fig. 3 (a) DSC scans of V_2O_5 : P_2O_5 as-made powders and milled V_2O_5. (b) XRD patterns of 75 : 25 V_2O_5 : P_2O_5 annealed at 313 °C and 450 °C. (c) Current densities (mA g^{-1}) before and after annealing at T_{c1} and 450 °C.

required; however, the focus of this work is a thorough analysis of the structure of the amorphous cathode and the implications towards improved electrochemical activity.

We undertook a variety of analytical techniques to isolate and understand the role of vanadium and phosphorous in the cathodes. Fig. 2a is the V L-edge Near-Edge X-ray Absorption Fine Structure (NEXAFS) comparing the electronic structure of the V 3d levels in V_2O_5 and V_2O_5 : P_2O_5 amorphous cathodes. Milled V_2O_5 exhibits three peaks (V1–V3) in the L_3 region ($2p_{3/2} \rightarrow 3d$) between 514–520 eV in addition to a broad peak in the L_2 region ($2p_{1/2} \rightarrow 3d$) between 522–528 eV. In accordance with the NEXAFS and XRD pattern (Fig. S2, ESI†), the milling of V_2O_5 did not alter the structure of the material, but only served to reduce the grain size. On the other hand, with the addition of the P_2O_5, the appearance of a new peak (V4) in addition to the characteristic peaks for V_2O_5 is observed. The presence of V4 resonates well with the V 2p X-ray photoelectron spectroscopy (XPS) comparing the powdered, milled and V_2O_5 : P_2O_5 (75 : 25) electrodes (Fig. S3, ESI†). The addition of the network-former serves to reduce the vanadium to a mix of $V^{4+/5+}$ oxidation state, which coincides with the loss of oxygen we observe with energy dispersive X-ray spectroscopy (Fig. S4, ESI†). Previous researchers have hypothesized that amorphization results in re-orientation of the V_2O_5 sheets to accommodate the inclusion of PO_4 units.[23] Additionally, calculations show that atomic vacancies are most favorably created at the terminally-bonded, apexial oxygen,[24] and are likely replaced by the PO_4 units. As the percentage of P_2O_5 (and presumably the PO_4) increases up to 75 : 25 mol%, there is a convergence of the V L_3 peaks. Our hypothesis is the loss of peak structure is reflected by the higher quantity of V^{4+} sites and PO_4 units resulting in improved vitrification. However beyond a 25 mol% of P_2O_5, there is a divergence of the L_3 region into separate peaks, and the presence of a new peak, V5, at 514.5 eV. It is clear that the changes to the parent V_2O_5 are linked to the role(s) of P_2O_5.

To observe the changes in the environment around the phosphorous, we performed ^{31}P MAS NMR (Fig. 2b). From 15% $\leq$ P_2O_5 $\leq$ 25%, there is a single peak located at −12 ppm (Peak 1, the additional peaks are spinning side-bands). The position of the peak relative to the standard H_3PO_4 evidences the formation of the PO_4 subunits during the mechanical milling synthesis, and the local environment around the phosphorous remains unchanged up to the 75 : 25 ratio in V_2O_5 : P_2O_5. Upon further addition of P_2O_5 up to 40 mol%, a shoulder at −5 ppm (Peak 2) reveals a separate environment of the phosphorous in the amorphous powder, which coincides with a small upfield shift for Peak 1. Interestingly, the current density and capacity of the cathodes increases to a maximum at 25% P_2O_5 and decreases thereafter, which implies that the addition of P_2O_5 beyond 30 mol% has a detrimental effect on the magnesiation of the cathode.

Crystallization of the amorphous powders provides crucial links to electrochemical performance.[25] Fig. 3a is the heating profile from differential scanning calorimetry (DSC) comparing V_2O_5 and the V_2O_5 : P_2O_5 powders. We would like to note that we did not observe any additional heat flow in the reverse scans for the DSC, and the structural changes due to heating are irreversible. A complete schedule for DSC measurements can be found in the ESI.† All of the amorphous materials exhibit a glass-transition temperature (T_g), suggesting that the milling of the reactants generates a glassy state. The stability of the amorphous material is defined as the difference in temperatures (ΔT) between the 1st crystallization peak (T_{c1}) and T_g, $\Delta T = T_{c1} - T_g$. The value of T_g increases with P_2O_5 content, and at the same time, the value of ΔT tends to increase. Since P_2O_5 is a network former, it is reasonable that high content of P_2O_5 can easily stabilize a glassy state. For 75 $\leq$ V_2O_5 $\leq$ 85 mol%, we observe the presence of two exothermic peaks. The presence of two crystallization (T_{c1} and T_{c2}) events after the T_g implies that metastable crystallites can be accessed from the pristine amorphous material by annealing at the first crystallization temperature, T_{c1}. On the other hand, for 60 $\leq$ V_2O_5 $\leq$ 70 mol%, the calorimetry displays only the presence of one peak after the glass transition temperature. The values of T_g, T_{c1}, T_{c2} and ΔT are listed in Table S1 of the ESI.† The calorimetry suggests that the

first crystallization, T_{c1}, differs with P_2O_5 content, suggesting that a more metastable phase can be thermally isolated. Representative SEM images of the annealed powders are shown in Fig. S5a–d (ESI†) for 75 : 25 and 60 : 40, respectively. For $75 \leq V_2O_5 \leq 85$ mol%, annealing the powders at T_{c1} triggers the formation of crater-like features due to the densification of the amorphous material and the subsequent crystallization at the base of the crater. When annealed at 450 °C, the formation of needle-like crystallites is observed in addition to the craters. Conversely, the $60 \leq V_2O_5 \leq 70$ mol% V_2O_5 shows a reversed crystallization order. XRD (Fig. S6, ESI†) shows how the crystallization of an apparent orthorhombic V_2O_5 phase coincides with the formation of the craters; while the needle-like structures are the formation of the various $VOPO_4$ phases. Fig. 3b displays the XRD patterns of the (001) crystallographic plane for the reactant V_2O_5 powder and a 75 : 25 V_2O_5 : P_2O_5 amorphous powder annealed at $T = 313$ °C (T_{c1}) and 450 °C. When precipitated from the amorphous powder at the first crystallization temperature, T_{c1}, the inter-layer spacing has increased as evidenced by the shift in peak position to $2\theta = 20.10^\circ$.

Crystallization has afforded insights into the active structural unit in of V_2O_5–P_2O_5 cathodes, however, precipitation from the amorphous phase does not yield a cathode with superior performance. Crystallization of amorphous Li_2S : P_2S_5 solid-state ionic conductors helps the precipitation of superionic crystals, resulting in lowering of the activation energy and increasing of the conductivity for Li^+ ion diffusion.[26] The electrochemical results for the precipitated phases show that the formation of $VOPO_4$, at 450 °C for $P_2O_5 \leq 25$ mol% and at T_{c1} for $P_2O_5 \geq 25$ mol%, consistently reduces the electrochemical activity of the cathode (Fig. 3c). Therefore, the 75 : 25 ratio strikes a balance between obtaining the maximum amount of the active, metastable phase, without producing the inactive $VOPO_4$ phase. The improved electrochemical activity due to the amorphization of the parent structure is further highlighted by the electrical conductivity of the 75 : 25 V_2O_5–P_2O_5 (1.7×10^{-8} S cm^{-1} @ 25 °C) in comparison to crystalline V_2O_5 (1.1×10^{-5} S cm^{-1} @ 25 °C). In accordance with previous studies, amorphous materials have much lower electronic conductivities than crystalline materials.[27,28] Thus the improved electrochemical activity is a consequence of the increased interlayer spacing. Additionally, when a V–O–P bond is formed in place of an apexial oxygen, charge compensation dictates that there will be two V^{4+} for each PO_4 unit as well as increasing the ionic character of the V–O–P bond. Scanlon *et al.*[24] recently showed that the oxygen vacancy at the apexial position can displace the V^{4+} in the (001) direction towards the underlying layer and localize the charge on the surrounding vanadium atoms. The "clustering" of charges has been to shown to promote Mg^{2+} diffusion, as shown for Mo_6 units in Chevrel Mo_6S_8 and recently C_{60}.[8,29]

In conclusion, when compared to poly-crystalline V_2O_5, the amorphous V_2O_5 : P_2O_5 cathodes show improved high-voltage electrochemical magnesiation. However, the reversibility, stability and battery voltage must still be explored through full-battery cell testing, therefore non-corrosive, high-voltage electrolytes compatible with magnesium metal remains an essential piece of the puzzle. Importantly, the results provide an exciting path to achieve high energy magnesium batteries.

Notes and references

1 D. Aurbach, Z. Lu, A. Schechter, Y. Gofer, H. Gizbar, R. Turgeman, Y. Cohen, M. Moshkovich and E. Levi, *Nature*, 2000, **407**, 724.
2 T. D. Gregory, R. J. Hoffman and R. C. Winterton, *J. Electrochem. Soc.*, 1990, **137**, 775.
3 D. Aurbach, I. Weissman, Y. Gofer and E. Levi, *Chem. Rec.*, 2003, **3**, 61.
4 J. Muldoon, C. B. Buccur and T. Gregory, *Chem. Rev.*, 2014, **114**, 1683.
5 R. E. Doe, R. Han, J. Hwang, A. J. Gmitter, I. Shterenberg, H. D. Yoo, N. Pour and D. Aurbach, *Chem. Commun.*, 2014, **50**, 243.
6 T. J. Carter, R. Mohtadi, T. S. Arthur, F. Mizuno, R. Zhang, S. Shirai and J. W. Kampf, *Angew. Chem., Int. Ed.*, 2014, **53**, 1.
7 Y. Cheng, T. Liu, Y. Shao, M. H. Engelhard, J. Liu and G. Li, *J. Mater. Chem. A*, 2014, **2**, 2473.
8 E. Levi, Y. Gofer and D. Aurbach, *Chem. Mater.*, 2010, **22**, 860.
9 C. Ling and F. Mizuno, *Chem. Mater.*, 2013, **25**, 3062.
10 Y. Cheng, L. R. Parent, Y. Shao, C. Wang, V. L. Sprenkle, G. Li and J. Liu, *Chem. Mater.*, 2014, **26**, 4904.
11 G. Gershinsky, H. D. Yoo, Y. Gofer and D. Aurbach, *Langmuir*, 2013, **29**, 10964.
12 Y. Liang, R. Feng, S. Yang, H. Ma, J. Liang and J. Chen, *Adv. Mater.*, 2011, **23**, 640.
13 Y. NuLi, J. Yang, J. Wang and Y. Li, *J. Phys. Chem. C*, 2009, **113**, 12594.
14 Y. J. Kim, W. Wu, S.-E. Chun, J. F. Whitcare and C. J. Bettinger, *Adv. Mater.*, 2014, **26**, 6572.
15 T. A. Arthur, R. Zhang, C. Ling, P.-A. Glans, X. Fan, J. Guo and F. Mizuno, *ACS Appl. Mater. Interfaces*, 2014, **6**, 7004.
16 V. Petkov, P. Y. Zavalij, S. Lutta, M. S. Whittingham, V. Parvanov and S. Shastri, *Phys. Rev. B: Condens. Matter Mater. Phys.*, 2004, **69**, 85410.
17 G. G. Amatucci, F. Badway, A. Singhal, B. Beaudoin, G. Skandan, T. Bowmer, I. Plitza, N. Pereira, T. Chapman and R. Jaworski, *J. Electrochem. Soc.*, 2001, **148**, A940.
18 P. Novàk and J. Desilvestro, *J. Electrochem. Soc.*, 1993, **140**, 140.
19 J. Song, M. Noked, E. Gillette, J. Duay, G. Rubloff and S. B. Lee, *Phys. Chem. Chem. Phys.*, 2015, **17**, 5256.
20 Y. Sakurai and J. Yamaki, *J. Electrochem. Soc.*, 1985, **132**, 512.
21 G. Delaizir, V. Seznec, P. Rozier, C. Surcin, P. Salles and M. Dolle, *Solid State Ionics*, 2013, **237**, 22.
22 B. Zhou, H. Shi, R. Cao, X. Zhang and Z. Jiang, *Phys. Chem. Chem. Phys.*, 2014, **16**, 18578.
23 F. R. Landsberger and P. J. Bray, *J. Chem. Phys.*, 1970, **53**, 2757.
24 D. O. Scanlon, A. Walsh, B. J. Morgan and G. W. Watson, *J. Phys. Chem. C*, 2008, **112**, 9903.
25 C. B. Carter and M. G. Norton, *Ceramic Materials and Engineering*, Springer, New York, NY, 2007.
26 F. Mizuno, A. Hayashi, K. Tadanaga and M. Tatsumisago, *Adv. Mater.*, 2005, **17**, 918.
27 F. Coustier, J. Hill, B. B. Owens, S. Passerini and W. H. Smyrl, *J. Electrochem. Soc.*, 1999, **146**, 1355.
28 L. Murawski, C. Gledel, C. Sanchez, J. Livage and J. P. Audieres, *J. Non-Cryst. Solids*, 1987, **89**, 98.
29 R. Zhang, C. Ling and F. Mizuno, *Chem. Commun.*, 2015, **51**, 1108.

